



## Importance of the structural integrity of a carbon conjugated mediator for photocatalytic hydrogen generation from water over a CdS–carbon nanotube–MoS<sub>2</sub> composite

Molly Meng-Jung Li, Poppy Mills, Simon M. Fairclough, Alex Robertson, Yung-Kang Peng, Jamie Warner, Chunyang Nie, Emmanuel Flahaut, Shik Chi Edman Tsang

### ► To cite this version:

Molly Meng-Jung Li, Poppy Mills, Simon M. Fairclough, Alex Robertson, Yung-Kang Peng, et al.. Importance of the structural integrity of a carbon conjugated mediator for photocatalytic hydrogen generation from water over a CdS–carbon nanotube–MoS<sub>2</sub> composite. Chemical Communications, 2016, 52 (93), pp.13596-13599. 10.1039/c6cc07632g . hal-02442132

**HAL Id: hal-02442132**

**<https://hal.science/hal-02442132>**

Submitted on 16 Jan 2020

**HAL** is a multi-disciplinary open access archive for the deposit and dissemination of scientific research documents, whether they are published or not. The documents may come from teaching and research institutions in France or abroad, or from public or private research centers.

L'archive ouverte pluridisciplinaire **HAL**, est destinée au dépôt et à la diffusion de documents scientifiques de niveau recherche, publiés ou non, émanant des établissements d'enseignement et de recherche français ou étrangers, des laboratoires publics ou privés.





## Open Archive Toulouse Archive Ouverte (OATAO)

OATAO is an open access repository that collects the work of Toulouse researchers and makes it freely available over the web where possible

This is a Publisher's version published in: <http://oatao.univ-toulouse.fr/16749>

**Official URL:** <http://dx.doi.org/10.1039/c6cc07632g>

### To cite this version:

Meng-Jung Li, Molly and Mills, Poppy and Fairclough, Simon M. and Robertson, Alex and Peng, Yung-Kang and Warner, Jamie and Nie, Chunyang  and Flahaut, Emmanuel  and Edman Tsang, Shik Chi [\*Importance of the structural integrity of a carbon conjugated mediator for photocatalytic hydrogen generation from water over a CdS–carbon nanotube–MoS<sub>2</sub> composite.\*](#) (2016) Chemical Communications, 52 (93). 13596-13599. ISSN 1359-7345

Any correspondence concerning this service should be sent to the repository administrator: [tech-oatao@listes-diff.inp-toulouse.fr](mailto:tech-oatao@listes-diff.inp-toulouse.fr)



Cite this: *Chem. Commun.*, 2016, 52, 13596

Received 20th September 2016,  
Accepted 19th October 2016

DOI: 10.1039/c6cc07632g

www.rsc.org/chemcomm

# Importance of the structural integrity of a carbon conjugated mediator for photocatalytic hydrogen generation from water over a CdS–carbon nanotube–MoS<sub>2</sub> composite†

Molly Meng-Jung Li,<sup>a</sup> Poppy Mills,<sup>a</sup> Simon M. Fairclough,<sup>‡a</sup> Alex Robertson,<sup>b</sup> Yung-Kang Peng,<sup>a</sup> Jamie Warner,<sup>b</sup> Chunyang Nie,<sup>c</sup> Emmanuel Flahaut<sup>c</sup> and Shik Chi Edman Tsang<sup>\*a</sup>

**Incorporation of CdS quantum dots is shown to significantly promote photocatalytic hydrogen production from water over single-layer MoS<sub>2</sub> in a remote manner via their dispersions on a carbon nanotube as a nanocomposite: the hydrogen evolution rate is found to be critically dependent on the content and structural integrity of the carbon nanotube such that the double-walled carbon nanotube shows superior H<sub>2</sub> production to a single-walled carbon nanotube because the inner carbon tubules survive from the structural damage during functionalization.**

The depletion of fossil fuel reserves and the undeniable environmental harm caused by their overconsumption make photocatalytic H<sub>2</sub> production from water attractive as a future renewable energy source.<sup>1,2</sup> Typically, photocatalytic splitting of water requires semiconductors to capture a photon with energy equal to or greater than their band gap energy. The photons are absorbed by a semiconductor nanocrystal, causing the generation of photo-excited electrons and holes in the conduction and valence bands, respectively. The excited electron-hole pairs, known as excitons, are then subjected to two main competitive deactivation routes, namely exciton recombination and exciton separation followed by chemical reactions. The former route is undesirable in photocatalysis, since this only emits heat or light with no chemical process involved, whereas the latter is important for photocatalytic reduction of water to hydrogen gas.

Nanosize CdS is a quantum dot material for efficient capture and emission of photons due to its characteristic band edges and band gap.<sup>3,4</sup> However, it displays very poor photocatalytic

activity due to rapid exciton recombination.<sup>5,6</sup> On the other hand, molybdenum disulfide (MoS<sub>2</sub>) is not an intrinsically active semiconductor to capture photons in photo-catalysis but its conduction band (−0.12 eV vs. NHE) and valence band (1.78 eV vs. NHE) render it suitable for electrochemical water-splitting.<sup>7</sup> It has been reported that an intimate CdS/MoS<sub>2</sub> mixture can catalyze photocatalytic H<sub>2</sub> evolution efficiently.<sup>8</sup> In addition, CdS supported on carbon materials is also proven to suppress charge recombination and provide active adsorption sites, which leads to the enhancement of photocatalytic activity.<sup>9–13</sup> Furthermore, the use of graphene to support CdS quantum dots and single layer MoS<sub>2</sub> (s-MoS<sub>2</sub>) appears to give a higher hydrogen evolution rate.<sup>7</sup> The functional roles of each component in these composite mixtures and their synergistic effect(s) for photocatalytic H<sub>2</sub> evolution are not yet clear. It is believed that by elucidating such material interactions, a rational design of composite materials for more efficient photocatalytic conversion into chemicals could be developed.

Here we report the systematic study of correlation of the photocatalytic H<sub>2</sub> activity with the structural and electronic properties of CdS and s-MoS<sub>2</sub> and interactions with surface functionalized single, double and multi-walled carbon nanotubes (SWNTs, DWNTs and MWNTs) (see the ESI†) in composites using a range of characterization techniques including XRD, TEM, SAED and Raman. In particular, the time-resolved photoluminescence (TRPL) technique is invoked to investigate the lifetime of excitons with reference to activity measured for this type of composite. It is found that the exciton recombination that readily takes place on CdS upon light activation can be effectively quenched when it is mixed with carbon nanotubes (CNTs) due to rapid transfer of the photo-excited electrons to the carbon structure before the proton reduction from water for the hydrogen production over s-MoS<sub>2</sub>. Thus, the light capturing sites (CdS) can be separated from hydrogen production sites (s-MoS<sub>2</sub>) via CNTs as electronic mediators. A higher hydrogen production rate is achieved over the two finely dispersed phases on the CNT than without the carbon structure due to its higher electron

<sup>a</sup> Wolfson Catalysis Centre, Department of Chemistry University of Oxford, Oxford, OX1 3QR, UK. E-mail: edman.tsang@chem.ox.ac.uk

<sup>b</sup> Department of Materials, University of Oxford, Oxford, OX1 3PH, UK

<sup>c</sup> Centre Interuniversitaire de Recherche et d'Ingénierie des Matériaux, Université Paul Sabatier, CIRIMAT, UMR CNRS 5085, Toulouse, France

† Electronic supplementary information (ESI) available: Supporting figures, and detailed experimental procedures, including XRD, TEM, FTIR, Raman, etc. See DOI: 10.1039/c6cc07632g

‡ Present address: Department of Physics, King's College London, UK.

conductivity and storage capacity.<sup>14,15</sup> It is also found that typical acid functionalization of CNTs for the immobilization of CdS and MoS<sub>2</sub> can lead to destruction of surface graphitic conjugation, affecting the essential process of electron transfer, which will lead to poor activity. As a result, DWNTs with intact inner carbon tubules act as optimal electron mediators for photocatalytic hydrogen production.

The powder XRD pattern of synthesised CdS quantum dots according to the literature is shown in Fig. S1(a) (ESI<sup>†</sup>), which confirms the CdS cubic structure. The Scherrer equation revealed an average particle size of 4.76 nm. This suggests small but uniform CdS nanoparticle size. The UV-visible absorption of CdS presented in Fig. S1(b) (ESI<sup>†</sup>) features an absorption hump at 472 nm corresponding to a reported band gap of 2.63 eV.<sup>3,4</sup> The TEM image also reveals typical 4.32 nm CdS nanoparticles and their size distribution is shown in Fig. S1(c) and (d) (ESI<sup>†</sup>). Single layer MoS<sub>2</sub> has also been synthesised (see the ESI<sup>†</sup>). Fig. S2 (ESI<sup>†</sup>) clearly shows that CdS nanoparticles tend to aggregate on the basal and edge regions of the restacked s-MoS<sub>2</sub> sheets with more than one monolayer thickness. The severe aggregation of CdS and s-MoS<sub>2</sub> at the material interface indicates a poor dispersion of these components for light capture and charge (exciton) separation. It was envisaged that dispersion of CdS and s-MoS<sub>2</sub> on high surface area CNTs may overcome the problems. Typical HNO<sub>3</sub> acid pre-treatment on CNTs has been applied for the removal of contaminants (such as amorphous carbon and catalyst particles) and also functionalization of the outer carbon structure with terminal carboxyl and hydroxyl groups for the immobilization and dispersion of a solid phase in the composite.<sup>16</sup> A detailed selection of acid treatments was reviewed, which revealed that most of the treatments can not only effectively remove contaminants but also cause shortening of tube length and functionalize the carbon surface.<sup>17</sup> Among various acids and concentrations applied, 3 M HNO<sub>3</sub> was regarded as the optimum concentration and served as a compromise between the yield of the functional groups created on CNTs and the chemical damage to the CNT structure. Therefore, the 3 M HNO<sub>3</sub> treatment was chosen for the CNT pre-treatment. The photocatalytic hydrogen production activity of the composite samples with lactic acid as the sacrificial reagent was measured. Fig. 1(a) shows that CdS or CdS/DWNTs are totally inert for the hydrogen production, implying that CdS and the CdS/DWNT interface cannot provide sites for proton reduction despite the well-known light capture ability for exciton production over the CdS and DWNT phases. In contrast, when s-MoS<sub>2</sub> is used, a significant quantity of H<sub>2</sub> is produced (137  $\mu\text{mol h}^{-1} \text{g}^{-1}$ ). Furthermore, the CdS/s-MoS<sub>2</sub> composite produces 1380  $\mu\text{mol h}^{-1} \text{g}^{-1}$  H<sub>2</sub>, which is clearly greater than CdS or s-MoS<sub>2</sub> alone.<sup>7</sup> There is a further increase in the amount of evolved H<sub>2</sub> gas when DWNTs are added to the CdS/s-MoS<sub>2</sub> (see E, F, G).

With an increased amount of DWNTs added, a maximum of H<sub>2</sub> gas is evolved (5728  $\mu\text{mol h}^{-1} \text{g}^{-1}$ ) at a 5 mg DWNT content. However, further increase in the amount of DWNTs could impair the photocatalytic H<sub>2</sub> production, presumably due to masking of active sites, *i.e.* the shielding effect,<sup>4</sup> when 7 mg of DWNTs is used. Upon comparing different forms of CNTs

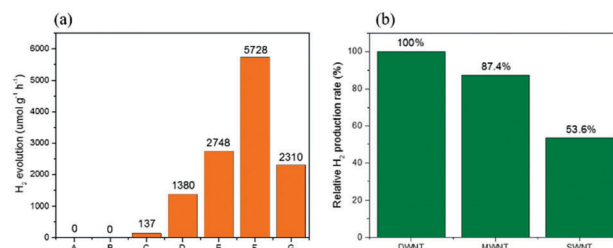


Fig. 1 (a) Hydrogen evolution rate for 20 mg of catalysts extracted from (A) CdS, (B) CdS/DWNT, (C) s-MoS<sub>2</sub>, (D) CdS/s-MoS<sub>2</sub>, (E) CdS/2 mg DWNT/s-MoS<sub>2</sub>, (F) CdS/5 mg DWNT/s-MoS<sub>2</sub>, and (G) CdS/7 mg DWNT/s-MoS<sub>2</sub>. (b) Hydrogen evolution rate for 5 mg of DWNTs; MWNTs and SWNTs to support CdS and s-MoS<sub>2</sub>.

(SWNTs, DWNTs and MWNTs) with the same loading, see Fig. 1(b), the DWNT composite gives the best activity on a per gram basis. Noticeably, the SWNT composite gives only half a H<sub>2</sub> production rate compared to the DWNT. As a result, the functional roles for each component particularly the nature and quality of CNTs as supports with respect to hydrogen production activity were investigated through careful material characterisation studies. To explore the charge (exciton) dynamics within the synthesised composites, the samples were examined using static and time-resolved photoluminescence spectroscopy (PL and TRPL). The steady-state PL spectra at an excitation wavelength of 405 nm shown in Fig. 2a contain anticipated strong emission from CdS quantum dots centred at 750 nm by recombination of excitons from the trap-state. However, CdS quantum dots when mixed with either CNTs or s-MoS<sub>2</sub> or CNT/s-MoS<sub>2</sub> exhibit much smaller trap-state peaks compared with CdS alone, suggesting that the radiative recombination of excitons in CdS is minimised. CNTs appear to be more effective in quenching the PL than MoS<sub>2</sub> on the same weight basis but the CdS/DWNT/s-MoS<sub>2</sub> mixture is the most effective. Fig. 2b shows the effectiveness

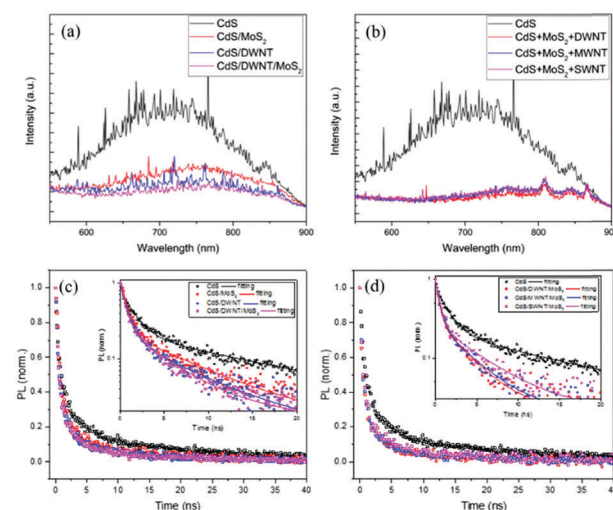


Fig. 2 Steady state PL, excitation 405 nm, for (a) CdS samples with different components and (b) CdS and CdS/CNT/s-MoS<sub>2</sub> samples. Time-resolved PL with decay monitored at 750 nm, excitation 405 nm, for (c) CdS samples with different components and (d) CdS and CdS/CNT/s-MoS<sub>2</sub> with different natures of CNTs.





**Table 1** The fractional contribution ( $f_i$ ) and lifetime ( $\tau_i$ ) of each decay component & average lifetime ( $\tau_{\text{avg}}$ ) for various samples

Material	$f_1$ (%)	$\tau_1$ (ns)	$f_2$ (%)	$\tau_2$ (ns)	$\tau_{\text{avg}}$ (ns)
CdS	20.8	1.45	79.2	16.03	13.00
CdS/MoS <sub>2</sub>	27.3	0.74	72.7	7.82	5.88
CdS/DWNT	30.9	0.79	69.1	6.83	4.97
CdS/DWNT/MoS <sub>2</sub>	28.4	0.64	71.6	3.96	3.02
CdS/MWNT/MoS <sub>2</sub>	33.9	0.89	66.1	4.72	3.42
CdS/SWNT/MoS <sub>2</sub>	26.8	0.79	73.2	5.90	4.53

of DWNTs, MWNTs and SWNTs in quenching the trap-state emission PL. From TRPL (Fig. 2c and d), an average lifetime ( $\tau$ ) for exciton recombination for each sample was derived and is shown in Table 1. The pristine CdS demonstrates an average lifetime of 13.00 ns; upon mixing with s-MoS<sub>2</sub> and DWNTs, the photo-generated carriers are indeed significantly quenched, where the DWNTs again show better quenching ability compared to s-MoS<sub>2</sub>. This indicates that the collection/extraction of photo-excited electrons from CdS to s-MoS<sub>2</sub> *via* DWNTs is more efficient than that of CdS/s-MoS<sub>2</sub>, presumably due to the electron storage and mobility of DWNTs. Among all the samples, CdS/DWNT/s-MoS<sub>2</sub> displays the lowest  $\tau$  (3.02 ns). Similar to the static PL, SWNTs (4.53 ns) are less effective than MWNTs (3.42 ns) and DWNTs (3.02 ns) in quenching the exciton emission. As MoS<sub>2</sub> is only the component to provide active sites for proton reduction to hydrogen (see Fig. 1), it is likely that the photoelectrons generated by CdS upon light excitation are quickly taken up by the CNTs before passing to s-MoS<sub>2</sub>. Apparently, the nature of CNTs appears to be critical for efficient transport and storage of photoelectrons from the CdS phase.

It is well known that the electronic properties of carbon nanotubes are crucially dependent on the diameter and chirality due to their distorted conjugated atomic tubular structure with partial overlap of Pz orbitals, whereas the electronic properties of MWNTs are quite complex, as each layer in the MWNTs can have different chiralities. Furthermore, MWNTs show considerably lower electronic conductivity than those of SWNTs or DWNTs because the interactions between the layers within MWNTs were found to disturb the electrical current along the tube axis.<sup>15</sup>

The morphology of DWNTs is very close to SWNTs, but the inner carbon tubes may provide detainment of the conjugation atomic pathway from aggressive mechanical or chemical damage to the outer tube surface.<sup>17</sup> High-resolution TEM (HR-TEM) images (Fig. 3a and b) thus show the raw single and double-walled CNTs with the tubular graphene feature for the SWNT and DWNT, respectively. After 3 M HNO<sub>3</sub> treatment, the majority of SWNTs are converted into carbon sheets and amorphous carbon (the area of serious destruction of SWNTs to amorphous carbon is shown in Fig. 3c). But many of the DWNTs retain their partially destructed tubular structure with amorphous carbon fragments (Fig. 3d). Thus, the more fragile nature of SWNTs leading to opening, unfolding and destruction to carbon fragments is particularly noted. Fig. S3 (a) (ESI†) shows the formation of new peaks of C=O stretching at 1691 cm<sup>-1</sup>, C=C and C=O at 1571 cm<sup>-1</sup> and C-O stretching at 1064 cm<sup>-1</sup> for the acid treated CNTs by FTIR spectroscopy. To quantify the global structural

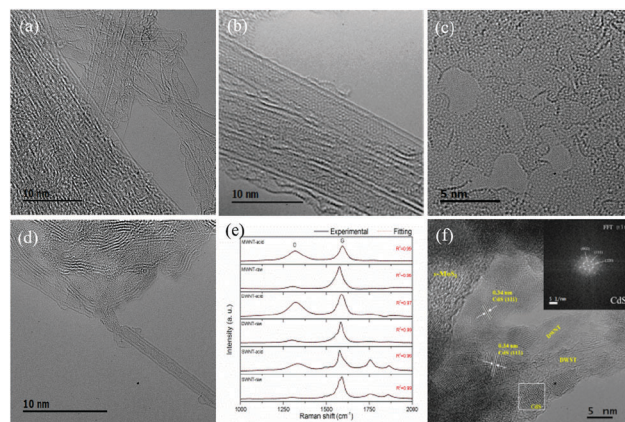
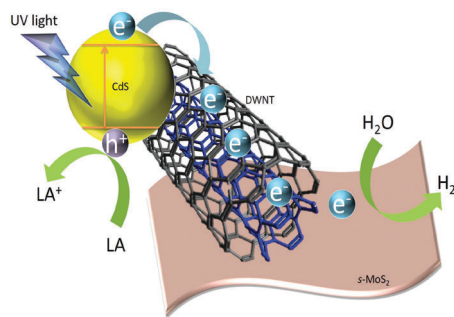


**Fig. 3** HR-TEM images of (a) raw SWNTs, (b) raw DWNTs, (c) acid-treated SWNTs, and (d) acid-treated DWNTs. (e) Raman spectra of raw CNTs and 3 M HNO<sub>3</sub> treated CNTs. (f) CdS/DWNT/s-MoS<sub>2</sub> (sheets) with inset of fast-Fourier transform (FFT) of CdS. The enlarged images are found in Fig. S2 (ESI†).

change of the samples before and after the same acid treatment, Raman spectra of raw and HNO<sub>3</sub>-treated CNTs are shown in Fig. 3e. The band located around 1315 cm<sup>-1</sup> is assigned to the D-band which is commonly associated with the disordered, sp<sup>3</sup>-hybridised carbon arising from defects and impurities, while the band located around 1580 cm<sup>-1</sup> is assigned to the G-band which is associated with the crystalline graphitic structures.<sup>18</sup> The intensity ratio of the D-band to the G-band is commonly used to quantify the degree of disorder in a graphene structure.<sup>19</sup> Generally, HNO<sub>3</sub>-treated CNTs showed larger D-band to G-band ratios, indicating the destruction of the graphene structure of CNTs during the acid treatment. Notably, the I<sub>D</sub>/I<sub>G</sub> ratio increases to 5.2 times in the SWNT, followed by 4.9 times in the DWNT and 2.1 times in the MWNT sample. The increase of the D-band ratio in SWNTs suggests that SWNTs indeed have undergone more serious damage after identical acid treatment (particularly on surfaces), which we believe impairs their charge transfer ability (larger  $\tau$  shown in Table 1), hence resulting in lower H<sub>2</sub> activity compared to DWNTs (see Fig. 1b). Fig. 3f shows that the image of the CdS/DWNT/s-MoS<sub>2</sub> composite, in which the regions of CdS nanoparticles and s-MoS<sub>2</sub> sheets dispersed on the partial tubular carbon structure can be differentiated through the corresponding lattice fringe distances and fast-Fourier transform (FFT) (inset of Fig. 3f). The intimate contact between CdS, s-MoS<sub>2</sub> and carbon nanotubes are clearly evidenced, which suggests that the CNTs remarkably decrease the aggregation of CdS and s-MoS<sub>2</sub> as they spread uniformly in the nanocomposite for superior H<sub>2</sub> activity compared to that without the carbon support. This indicates the future design of efficient photoactive composites for separation and optimization of light capture nanomaterials from catalytic hydrogen production materials *via* electron conductive mediators in a remote way. It is also clear from this study that the crucial maintenance of the integrity of the graphitic tubular structure and the intactness of the conjugation of inner tubes are imperatively important for the charge transport and storage from the light capture CdS phase to hydrogen production sites on s-MoS<sub>2</sub> for optimal photo-catalysis.





**Scheme 1** Photocatalytic production of hydrogen from water over CdS-carbon nanotube (CNT)-MoS<sub>2</sub> is found critically dependent on the content and nature of the nanotube used. Time resolved photo-luminescence indicates that the surface graphitic structure of the CNT is vulnerable to damage, halting the essential electron transfer for H<sub>2</sub> formation. Thus, the DWNT exhibits superior H<sub>2</sub> activity to the SWNT because of the structural integrity of the inner tubule.

In summary, photocatalytic hydrogen evolution activity through water splitting is greatly enhanced by the incorporation of carbon nanotubes and single-layered MoS<sub>2</sub> nano-sheets as cocatalysts into the CdS system. CdS/DWNT/s-MoS<sub>2</sub> with the optimal amount of DWNTs (mass ratio of CdS:DWNT:s-MoS<sub>2</sub> = 100:5:2) can provide a high hydrogen evolution rate of 5728  $\mu\text{mol g}^{-1} \text{h}^{-1}$ , and the unique roles of intact carbon nanotubes as electron mediators are for the first time identified by this present systematic TRPL study, as summarized in Scheme 1. In addition, a DWNT shows the best performance compared to other forms of CNTs, due to its robust double-walled structure, which can provide protection for the inner tube from surface damage during functionalization/handling, while a SWNT inevitably suffers from destruction of conjugation. This study depicts the importance of fabrication of intimate heterojunctions demonstrating the benefits of nano-ensembles of functional units for light

capture, carrier transfer and catalysis in synergy for efficient photo-production of hydrogen from water.

The financial supports of this work from the EPSRC of UK and the Royal Society international joint project with the carbon nanotube group (CNRS) at Toulouse, France, are acknowledged. MMJL acknowledges a Swire Scholarship for her DPhil study at Oxford University, U.K.

## Notes and references

- 1 M. Ni, M. K. Leung, D. Y. Leung and K. Sumathy, *Renewable Sustainable Energy Rev.*, 2007, **11**, 401–425.
- 2 A. Kudo and Y. Miseki, *Chem. Soc. Rev.*, 2009, **38**, 253–278.
- 3 X. Chen, S. Shen, L. Guo and S. S. Mao, *Chem. Rev.*, 2010, **110**, 6503–6570.
- 4 Q. Li, B. Guo, J. Yu, J. Ran, B. Zhang, H. Yan and J. Gong, *J. Am. Chem. Soc.*, 2011, **133**, 10878–10884.
- 5 A. Cao, Z. Liu, S. Chu, M. Wu, Z. Ye, Z. Cai, Y. Chang, S. Wang, Q. Gong and Y. Liu, *Adv. Mater.*, 2010, **22**, 103–106.
- 6 D. J. Fermin, E. A. Ponomarev and L. M. Peter, *J. Electroanal. Chem.*, 1999, **473**, 192–203.
- 7 T. Jia, A. Kolpin, C. Ma, R. C.-T. Chan, W.-M. Kwok and S. C. E. Tsang, *Chem. Commun.*, 2014, **50**, 1185–1188.
- 8 J. Zhang, Z. Zhu and X. Feng, *Chem. – Eur. J.*, 2014, **20**, 10632–10635.
- 9 I. Robel, B. A. Bunker and P. V. Kamat, *Adv. Mater.*, 2005, **17**, 2458–2463.
- 10 D. Lang, T. Shen and Q. Xiang, *ChemCatChem*, 2015, **7**, 943–951.
- 11 S. Pan and X. Liu, *New J. Chem.*, 2012, **36**, 1781–1787.
- 12 Q. Xiang, F. Cheng and D. Lang, *ChemSusChem*, 2016, **9**, 996–1002.
- 13 A. Ye, W. Fan, Q. Zhang, W. Deng and Y. Wang, *Catal. Sci. Technol.*, 2012, **2**, 969–978.
- 14 R. Baughman, A. Zakhidov and W. A. de Heer, *Science*, 2002, **297**, 787–792.
- 15 R. Saito, G. Dresselhaus and M. S. Dresselhaus, *Phys. Rev. B: Condens. Matter Mater. Phys.*, 1996, **53**, 2044–2050.
- 16 Y. Yao, G. Li, S. Ciston, R. M. Lueptow and K. A. Gray, *Environ. Sci. Technol.*, 2008, **42**, 4952–4957.
- 17 T. Bortolamiol, P. Lukanov, A.-M. Galibert, B. Soula, P. Lonchambon, L. Datas and E. Flahaut, *Carbon*, 2014, **78**, 79–90.
- 18 I. D. Rosca, F. Watari, M. Uo and T. Akasaka, *Carbon*, 2005, **43**, 3124–3131.
- 19 H. Murphy, P. Papakonstantinou and T. I. T. Okpalugo, *J. Vac. Sci. Technol., B: Microelectron. Nanometer Struct.–Process., Meas., Phenom.*, 2006, **24**, 715–720.



## Electronic Supporting Information

### Experimental details

#### 1. Catalyst preparation

##### 1.1 Materials

Reagents used throughout this thesis were purchased from Sigma Aldrich and were used without modification or purification unless stated: Cadmium Chloride-  $\text{CdCl}_2$  (99.99% trace metals basis), Oleylamine (technical grade, 70%), Sulfur (99.998% trace metals basis), Molybdenum Disulfide-  $\text{MoS}_2$  (99% 2H- $\text{MoS}_2$ ), n-Butyl Lithium (1.6 M solution in hexane), Hexane ( $97 \geq$  chromasolv for HPLC), Nitric Acid-  $\text{HNO}_3$  (ACS reagent), Lactic Acid (85%), SWNT (carbon  $>90\%$ ,  $\geq 80.0\%$  carbon as SWNT ( $\text{BET} \approx 560 \text{ m}^2\text{g}^{-1}$ ), 0.7-1.4 nm diameter). The DWNTs ( $345 \text{ m}^2\text{g}^{-1}$ ) were produced by catalytic chemical vapor deposition (CCVD) of a  $\text{H}_2$ - $\text{CH}_4$  mixture at  $1000^\circ\text{C}$  with CoMo-MgO catalyst.<sup>[1,2]</sup> MWNTs ( $369 \text{ m}^2\text{g}^{-1}$ ) were synthesized by Catalytic Chemical Vapour Deposition using a Co:Mo-MgO catalyst with an elemental composition of  $\text{Mg}_{0.9}\text{Co}_{0.033}\text{Mo}_{0.067}\text{O}$ . The catalyst was heated in an atmosphere containing 36% of  $\text{CH}_4$  and 64% of  $\text{H}_2$ , at a total flow-rate of 15L/h, starting from room temperature to  $1000^\circ\text{C}$  at  $5^\circ/\text{min}$ . No dwell was applied and the gaseous atmosphere was maintained constant during all the procedure.<sup>[3]</sup> CNTs are free from amorphous carbon coating. During the extraction process, oxides (unreacted CoMo-MgO) and unprotected metal nanoparticles (Co, Mo) were dissolved by addition of aqueous HCl solution. The acidic suspension was then filtered on  $0.45 \mu\text{m}$  pore-size polypropylene membranes and washed with deionized water until neutrality. The sample was freeze-dried.

##### 1.2 Synthesis of cadmium sulphide

The synthesis of CdS spherical NPs followed the method described by Joo et. al.<sup>[4]</sup> Firstly, 604 mg of cadmium chloride (3 mmol) was dissolved in 30 mL of oleylamine with the assistance of sonication and stirring using a magnetic stirrer bar. This solution was then heated to  $90^\circ\text{C}$  with constant stirring in a three-necked flask for 1 h in air. 48 mg of sulfur dissolved in 5 mL oleylamine was then injected into the mixture dropwise. The solution was then heated to  $160^\circ\text{C}$  under a  $\text{N}_2$  atmosphere and left for 6 h under vigorous stirring. After leaving to cool overnight, the nanoparticles were then collected using centrifugation (5000 rpm for 10 min) and were thoroughly washed with acetone five times to ensure all solvent and excess ligand had been removed.

##### 1.3 Synthesis of single-layer molybdenum disulphide (s- $\text{MoS}_2$ )

Single-layer  $\text{MoS}_2$  (s- $\text{MoS}_2$ ) was synthesised by the Tsang group following a well-documented route of exfoliation of bulk  $\text{MoS}_2$  with lithium intercalation.<sup>[5,6]</sup> Initially the black  $\text{MoS}_2$  powder was soaked for 48 h in 1.6 M solution of n-butyl lithium in hexane under  $\text{N}_2$  atmosphere. After this initial intercalation step of  $\text{MoS}_2$  with lithium, the  $\text{Li}_x\text{MoS}_2$  was then repeatedly washed with hexane to remove excess butyl lithium and dried under  $\text{N}_2$  atmosphere. The powder was then sonicated in DI water for 48 h to assist exfoliation. The reaction between water and intercalated lithium forms  $\text{H}_2$  between the layers and the gas expansion tends to separate the  $\text{MoS}_2$  layers until the layers become completely separated and

suspended in the aqueous solution. The product was filtered, washed extensively with water and ethanol and then dried under vacuum. Atomic force microscopy (AFM) image of the synthesised s-MoS<sub>2</sub> can be found in the reference no. 6 (summarised in Figure S5).

#### 1.4 Acid treatment of CNTs

Following a method reported by E. Flahaut et al.,<sup>[7]</sup> initially 200 mg of raw CNTs were placed into 200 mL 3M HNO<sub>3</sub> solution in a 500 mL pyrex flask and sonicated for 30 min then refluxed under vigorous stirring for 24 h at 130°C. The black suspension was then washed three times with 100 mL DI water before drying the product at 80°C in air overnight.

#### 1.5 Synthesis of CdS/CNT/s-MoS<sub>2</sub> nanocomposites

CdS/CNT/s-MoS<sub>2</sub> composites were synthesised using a modified CdS-graphene oxide-MoS<sub>2</sub> by T. Jia et al.<sup>[8]</sup> Initially, 100 mg CdS, 2 mg s-MoS<sub>2</sub> and acid treated CNTs (0.4, 2, 5 and 7mg) in 50 mL ethanol were sonicated for 4 h and then stirred at room temperature for a further 24 h. The suspensions were filtered using a 0.2 µm membrane and washed with 250 mL ethanol. The sample was then vacuum dried at 80°C in air overnight.

## 2. Catalyst characterizations

### 2.1 Transmission electron microscopy (TEM)

TEM images were taken using a JEOL 2100 Transmission Electron Microscope at 200 kV. The sample particles were deposited on an Agar Scientific Holey carbon supported copper 400 mesh grid. TEM samples were prepared by sonicating a suitable amount of material in 1 mL ethanol for 15 minutes before drop wise adding the solution onto the copper grid.

### 2.2 X-ray diffraction (XRD)

Powder X-ray profiles were obtained on a PANalytical X'Pert Pro Diffractometer by mounting a glass sample slide with the pressed powdered material onto a sample slide holder inside the diffractometer. The intensity of the diffracted beams was measured as a function of the 2θ angle, usually in the range of 10-80°.

### 2.3 Fourier transform infrared spectroscopy (FTIR)

FTIR spectra were acquired using a Nicolet 6700 ATR-IR spectrometer with a liquid-nitrogen-cooled detector. The solid samples were pressed onto the smart golden gate-ZeSe/diamond crystal. The spectra were obtained by averaging 128 scans with a resolution of 2 cm<sup>-1</sup> over the wavenumbers ranging from 1000-3500 cm<sup>-1</sup>.

### 2.4 Raman spectroscopy

Raman spectra were recorded using a Perkin-Elmer Raman Station 400. This instrument is a bench-top spectrometer with laser excitation wavelength at 785 nm and CCD detector. Powder samples were prepared by placing the powder on a glass slide.

### 2.5 Ultraviolet-visible absorption spectroscopy



UV-vis absorption spectra were taken using a Varian 100 Bio UV-Visible Spectrometer in absorbance mode in the range 200-800 nm with a step interval of 1 nm. Samples were prepared by sonicating 2 mg of sample in 10 mL ethanol for 15 minutes before putting the sonicated solution into an optical glass cuvette. Ethanol was thus used as the reference.

## 2.6 Steady-state and time-resolved photoluminescence spectroscopy

Steady-state and time-resolved photoluminescence (PL) measurements were acquired using a time-correlated single photon counting (TCSPC) setup (FluoTime 300, PicoQuant GmbH). Samples were excited using 405nm laser pulsed at frequencies of 40MHz (for steady state measurements) and 10MHz (for time-resolved measurements). The PL was collected using a high resolution monochromator and hybrid photomultiplier detector assembly (PMA Hybrid 40, PicoQuant GmbH). Parameters describing the photoluminescence were obtained by fitting the background-corrected PL with a decay equation of emission intensity  $I(\lambda, t)$  at the time ( $t$ ) and wavelength ( $\lambda$ ) of the form:

$$I(\lambda, t) = I_0(\lambda, t = 0) \sum a_i e^{-\frac{t}{\tau_i}}$$

Where  $\tau_i$  is the characteristic lifetime of the  $i$ th decay component,  $a_i$  is the subsequent decay amplitude, and  $I_0(\lambda)$  is the emission intensity at time  $t=0$ . Errors in the fitting parameters were determined by examining the adjusted r-squares obtained by independently varying each fitting parameter.

For ease of comparison of lifetimes between CdS samples with different cocatalysts, the intensity weighted average lifetime is given by:

$$\tau_{avg} = \frac{\sum a_i \tau_i^2}{\sum a_i \tau_i} = \sum f_i \tau_i$$

Where  $f_i$  is the fractional contribution of each decay components and the denominator is over all amplitudes and decay times which is proportional to the total intensity.<sup>[9]</sup>

For PL and TRPL measurements, a proportion of sample was extracted from the mixture: A: 100 mg CdS; B: CdS/DWNT (100 mg CdS + 5mg DWNT); C: CdS/s-MoS<sub>2</sub> (100 mg CdS + 2mg s-MoS<sub>2</sub>); D: CdS/5mg DWNT/s-MoS<sub>2</sub> (100 mg CdS + 5mg DWNT+ 2mg s-MoS<sub>2</sub>); E: CdS/5mg SWNT/s-MoS<sub>2</sub> (100 mg CdS + 5mg SWNT+ 2 mg s-MoS<sub>2</sub>); F: CdS/5mg MWNT/s-MoS<sub>2</sub> (100 mg CdS + 5mg MWNT+ 2 mg s-MoS<sub>2</sub>)

## 3. Photocatalytic testing

Photocatalytic H<sub>2</sub> evolution experiments were performed in a 500 mL sealed Pyrex flask at ambient temperature and atmospheric pressure. The reactor was positioned 10 cm away from the 500 W UV-vis lamp. In a typical photocatalytic experiment, 20 mg catalyst was suspended in 90 mL DI water and 10 mL lactic acid and sonicated for 30 min. Prior to irradiation, the suspension was bubbled with 5 % CH<sub>4</sub>/Ar for 15 min to remove the dissolved oxygen and to ensure the reaction was under anaerobic conditions, the CH<sub>4</sub> acted as an

internal reference for gas chromatography calibration. Continuous magnetic stirring was applied in order to keep the photocatalyst particles suspended during the irradiation. A 20 mL sample of the generated gas was collected and analysed by Agilent 7890A gas chromatography with TCD detector.

In the Figure 1 of the main manuscript, hydrogen evolution rate for 20 mg catalysts was taken from the mixture and measured. A: CdS (100 mg); B: CdS/DWNT (100 mg CdS +0.4g DWNT); C: s-MoS<sub>2</sub>; D: CdS/s-MoS<sub>2</sub> (100 mg CdS + 2 mg s-MoS<sub>2</sub>); E: CdS/2mg DWNT/s-MoS<sub>2</sub> (100 mg CdS +2mg DWNT+ 2 mg s-MoS<sub>2</sub>); F: CdS/5mg DWNT/s-MoS<sub>2</sub> (100 mg CdS +5mg DWNT+ 2 mg s-MoS<sub>2</sub>); G: CdS/7mg DWNT/s-MoS<sub>2</sub> (100 mg CdS +7mg DWNT+ 2 mg s-MoS<sub>2</sub>), etc.

## Supporting figures and tables

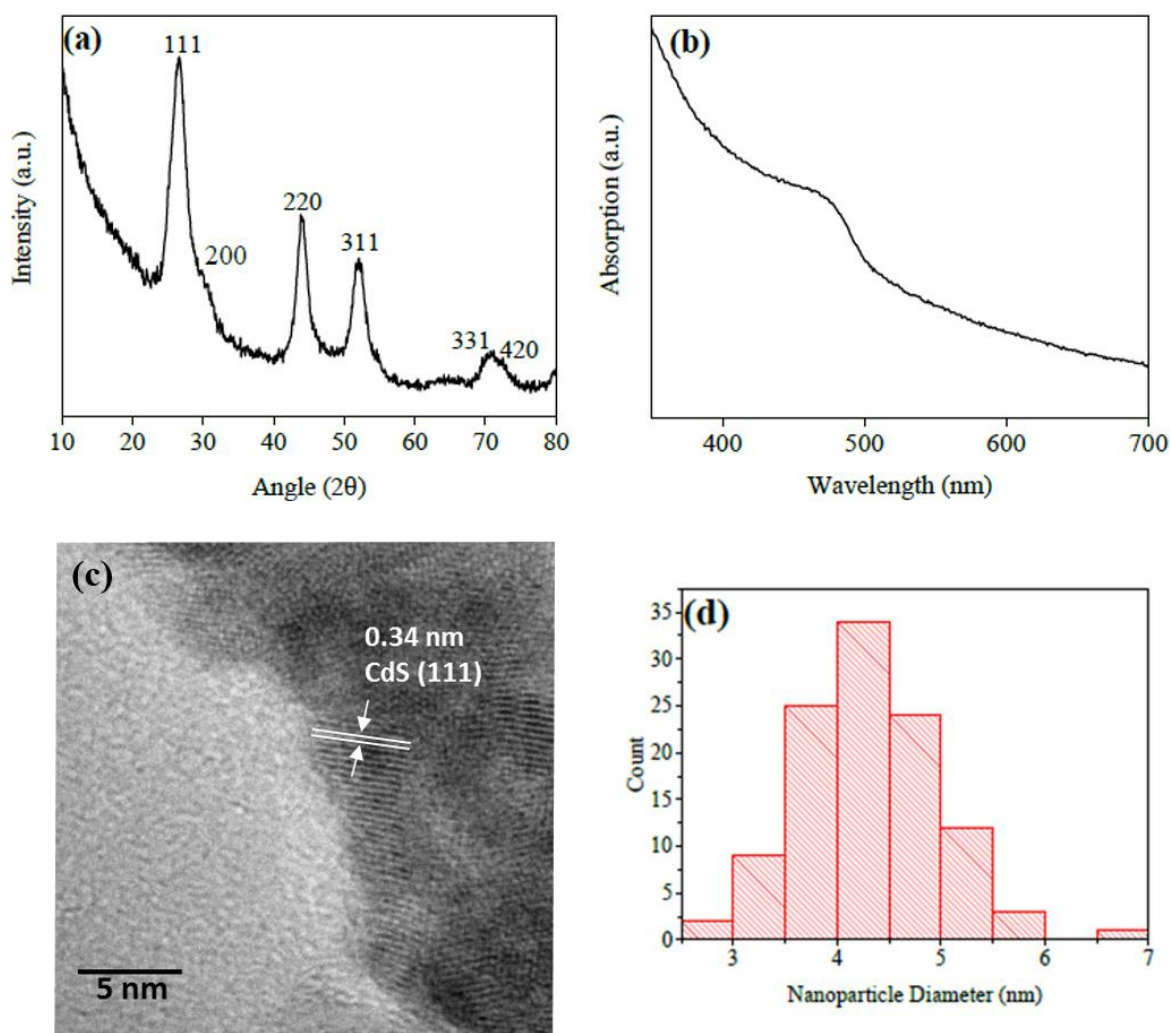


Figure S1 (a) X-ray diffraction pattern; (b) UV-visible absorption spectrum; (c) TEM image; (d) nanoparticle diameter size distribution of synthesised CdS nanoparticles.

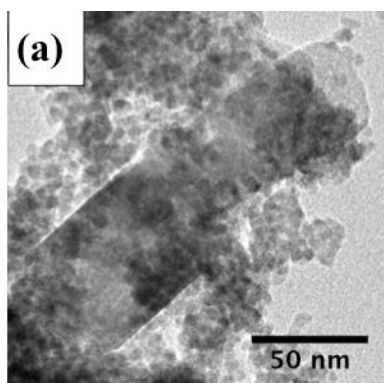


Figure S2A TEM image of CdS/*s*-MoS<sub>2</sub> nanocomposite, which reveals the aggregation of CdS nanoparticles on the basal planes and the edges of re-stacked *s*-MoS<sub>2</sub>.

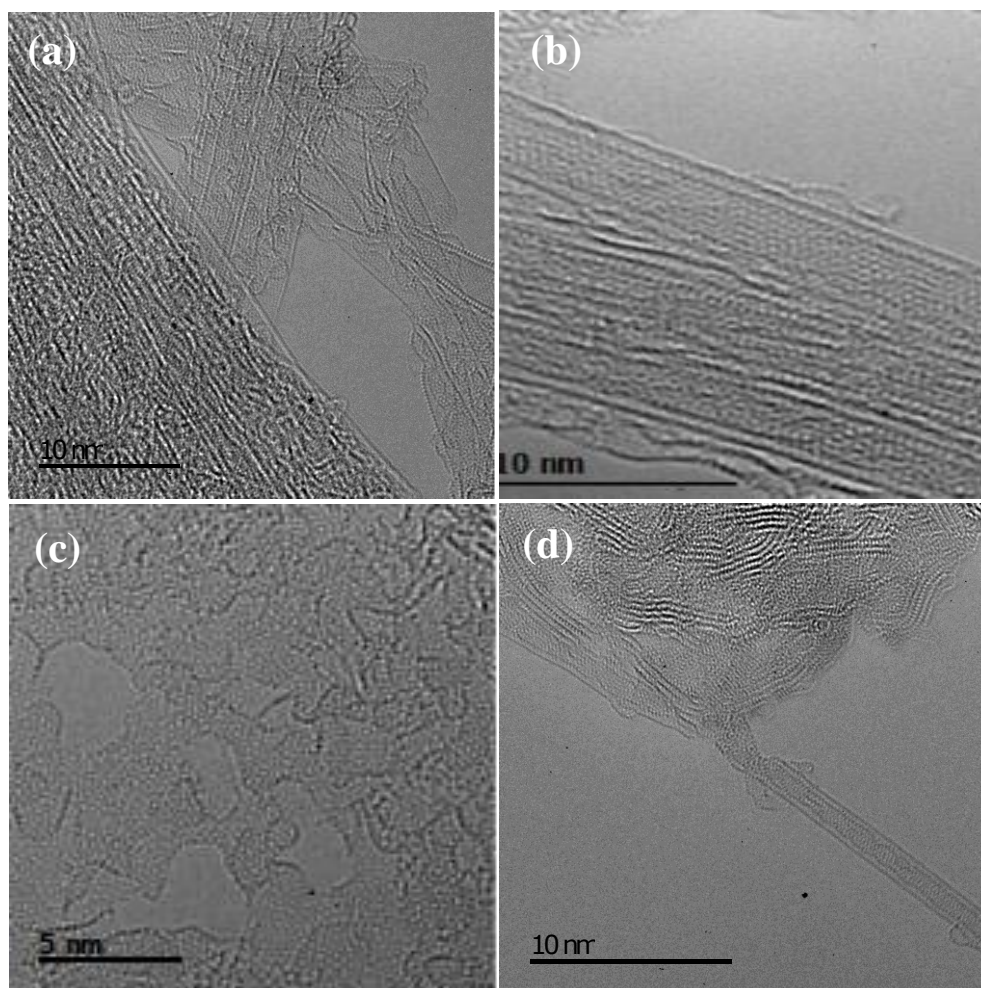


Figure S2B Typical HR-TEM images of (a) raw SWNT; (b) raw DWNT; (c) acid-treated SWNT; (d) acid-treated DWNT

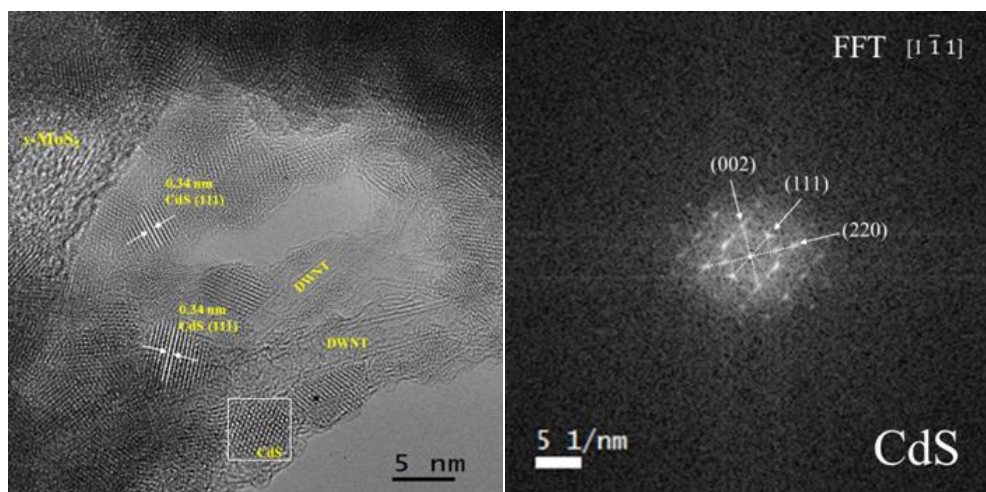


Figure S2C: Left: A typical HR-TEM image of CdS/DWNT/s-MoS<sub>2</sub>, the marked areas rich in compound(s) were confirmed by EDX; Right: Selected area of CdS nanoparticle with corresponding fast-Fourier Transform (FFT).

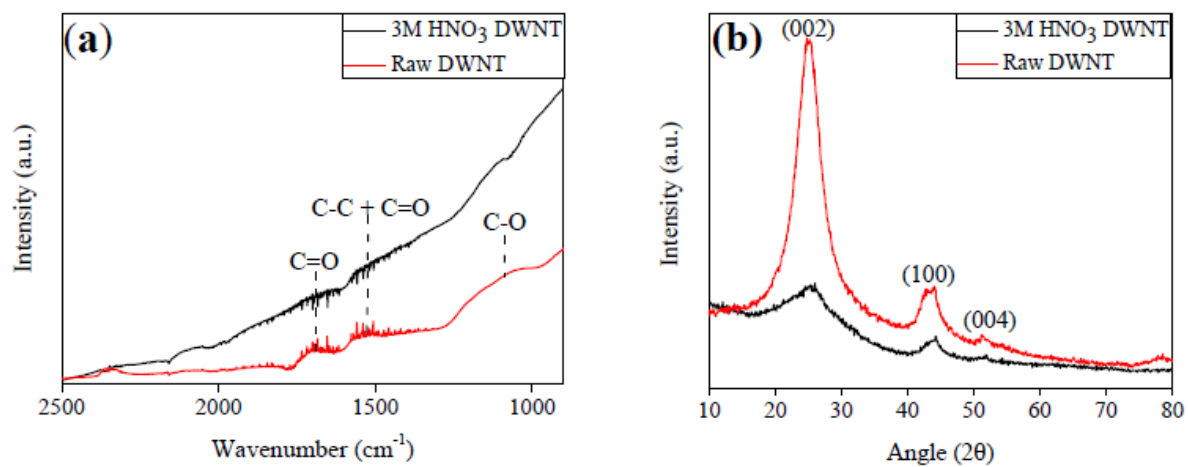


Figure S3 (a) FTIR, (b) XRD of 3M HNO<sub>3</sub> treated DWNT and raw DWNT.

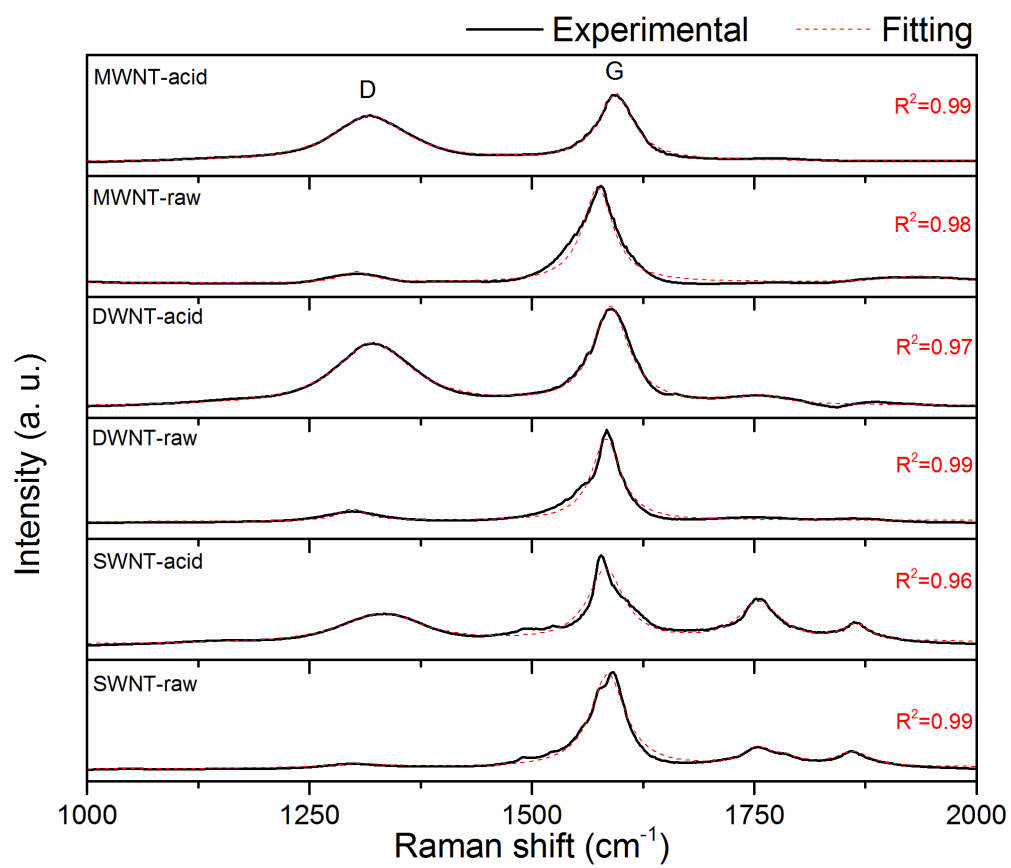


Figure S4 Raman spectra of raw CNTs and 3M HNO<sub>3</sub> treated CNTs.



Table S1 The  $A_D/A_G$  and  $I_D/I_G$  ratios of the raw and acid treated CNTs.

<b>Sample</b>	<b><math>A_D/A_G</math></b>	<b><math>I_D/I_G</math></b>
SWNT-raw	0.0261	0.0821
SWNT-Acid	1.431	0.4305
SWNT Ratio increment (acid/raw)	54.828	5.244
DWNT-raw	0.263	0.1404
DWNT-Acid	1.221	0.6894
DWNT Ratio increment (acid/raw)	4.643	4.910
MWNT-raw	0.0918	0.3490
MWNT-Acid	1.15	0.7265
MWNT Ratio increment (acid/raw)	12.527	2.082

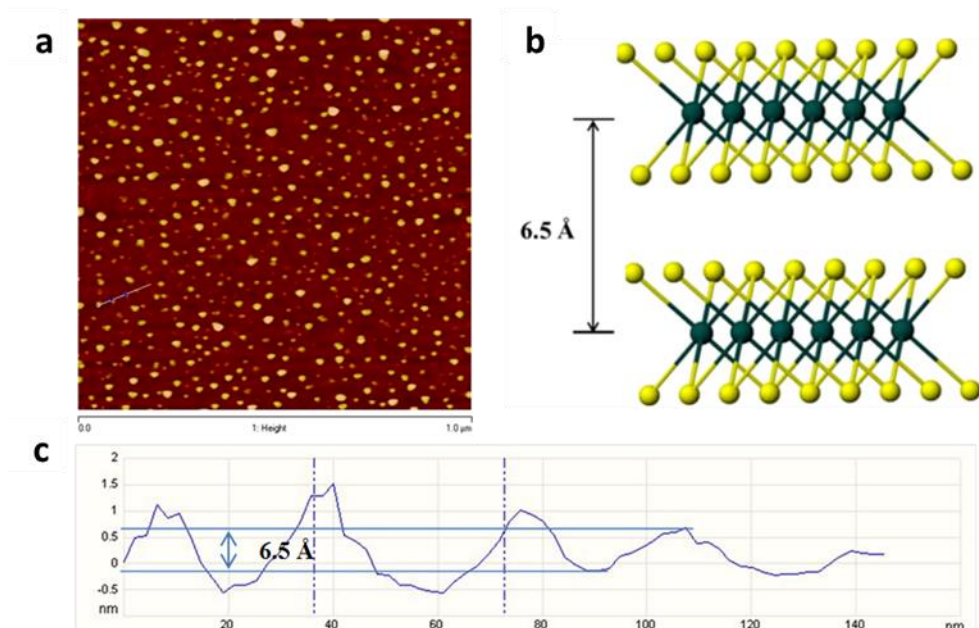


Figure S5 Atomic force microscopy (AFM) image analyses for the fresh chemically exfoliated s-MoS<sub>2</sub>- refer to reference <sup>6</sup> (a, AFM image of spin coated s-MoS<sub>2</sub> and b, a model of 2-H MoS<sub>2</sub> structure perpendicular to c axis, 100 flakes is scanned with majority of heights between 0.6-0.7nm. The sample was prepared by spin-coating s-MoS<sub>2</sub> onto a surface of Si/SiO<sub>2</sub> substrate. The lateral dimension of this s-MoS<sub>2</sub> nanosheet is approximately 20-40 nm. c, It can be seen that the step heights of individual layers of 0.6-0.7 nm. This value is comparable to ca. 0.65 nm of a single layer of the S-Mo-S building block. Statistical analysis of 100 flakes produced by the lithium exfoliation method revealed that 56% of the flakes to be monolayer, 28% of two layers and 13% of three layers and so on. The average topographic height is around 1.04 nm, which agrees with typical height of a s-MoS<sub>2</sub> with the presence of water molecules (between 0.6 and 1.0 nm).

### Photo-corrosion of CdS quantum dots on Carbon Nanotubes

It is well accepted that the competition reaction such as sulphide oxidation induced by the positive charged hole instead of carrying out the highly activated oxidation process of water molecule to oxygen and proton, can cause photo-corrosion of CdS semiconductor. However, photocatalytic hydrogen production from the reduction of proton in solution over the defined material components was the main focus of this work, we had thus tried to avoid the issue of photo-corrosion. Using a reducing agent used as the hole scavenger in aqueous solution is a well-known strategy to stabilize CdS from the photo-corrosion. In this study, lactic acid was therefore used as the sacrificial reagent to suppress the photo-corrosion of CdS with the lactic acid preferentially oxidised into pyruvic acid. Thus, in this system, we did not evaluate the extent of photo-corrosion of CdS quantum dots with or without CNTs (we did not encounter this problem by using lactic acid as the sacrificial reductant). On the other hand, the high surface area CNTs with high intrinsic electronic conductivity, are expected to reduce the local positively charge (hole) built up over the CdS quantum dots together with higher

concentration of adsorbed lactic acid, that can in principle greatly reduce the extent of photo-corrosion. However, these anticipations should be carefully verified.

## References

1. E. Flahaut, R. Bacsá, A. Peigney, C. Laurent, *Chem. Commun.* **2003**, 12, 1442-1443.
2. E. Flahaut, A. Peigney, W. S. Bacsá, R. R. Bacsá and Ch. Laurent, *J. Mater. Chem.* **2004**, 14, 646-653.
3. L. García- Hevia, R. Valiente, J. L. Fernández-Luna, E. Flahaut, L. Rodríguez-Fernández, J. C. Villegas, J. González, M. L. Fanarraga, *Adv. Health Mater.* **2015**, 4, (11), 1640–1644.
4. J. Joo, H. B. Na, T. Yu, J. H. Yu, Y. W. Kim, F. Wu, J. Z. Zhang, T. Hyeon, *J. Am. Chem. Soc.* **2003**, 125, 11100-11105.
5. P. Joensen, R. F. Frindt, S. R. Morrison, *Mat. Res. Bull.* **1986**, 21, 457-461.
6. T. Jia, M. M. J. Li, L. Ye, S. Wiseman, G. Liu, J. Qu, K. Nakagawa, S. C. E. Tsang, *Chem. Commun.* **2015**, 51, 13496-13499.
7. T. Bortolamiol, P. Lukanov, A-M. Galibert, B. Soula, P. Lonchambon, L. Datas, E. Flahaut, *Carbon* **2014**, 78, 79-90.
8. T. Jia, A. Kolpin, C. Ma, R. C.-T. Chan, W.-M. Kwok, S. C. E. Tsang, *Chem. Commun.* **2014**, 50, 1185-1188.
9. J. Seo, R. Fudala, W. J. Kim, R. Rich, B. Tabibi, H. Cho, Z. Gryczynski, I. Gryczynski, W. Yu, *Opt Mater Express* **2012**, 2, 1026-1039.